Geophysical Journal International

Geophys. J. Int. (2020) **220,** 1187–1196
Advance Access publication 2019 November 15
GJI General Geophysical Methods

doi: 10.1093/gji/ggz515

Effect of solute concentration on the spectral induced polarization response of calcite precipitation

Satoshi Izumoto [1], Johan Alexander Huisman [1], Yuxin Wu [2] and Harry Vereecken [1]

[1] *Agrosphere (IBG 3), Institute of Bio- and Geosciences, Forschungszentrum Jülich, Jülich, Germany. E-mail: s.izumoto@fz-juelich.de*
[2] *Earth and Environmental Sciences Area, Lawrence Berkeley National Laboratory, Berkeley, CA, USA*

Accepted 2019 November 13. Received 2019 November 10; in original form 2019 June 28

SUMMARY

Induced calcite precipitation is used in geotechnics to modify the mechanical and hydrological properties of the underground. Laboratory experiments have shown that spectral induced polarization (SIP) measurements can detect calcite precipitation. However, the results of previous studies investigating the SIP response of calcite precipitation were not fully consistent. This study aims to investigate how the SIP response of calcite depends on solute concentration to explain the differences in SIP response observed in previous studies. A four-phase experiment with SIP measurements on a column filled with sand was performed. In phase I, calcite precipitation was generated for a period of 12 d by co-injecting Na_2CO_3 and $CaCl_2$ solutions through two different ports. This resulted in a well-defined calcite precipitation front, which was associated with an increase in the imaginary part of the conductivity (σ''). In phase II, diluted solutions were injected into the column. This resulted in a clear decrease in σ''. In phase III, the injection of the two solutions was stopped while calcite precipitation continued and solute concentrations in the mixing zone decreased. Again, this decreased σ''. Finally, the injection rate of the Na_2CO_3 solution was reduced relative to that of the $CaCl_2$ solution in phase IV. This resulted in a shift of the mixing zone away from the calcite precipitation front established in phase I and an associated decrease of σ''. These results imply that the SIP response of calcite is highly sensitive to the solute concentration near the precipitates, which may explain previously reported conflicting results.

Key words: Electrical properties; Microstructure; Permeability and porosity; Hydrogeophysics.

1 INTRODUCTION

Precipitation and dissolution dynamics of calcite in response to variations in groundwater pH and alkalinity are important in a range of subsurface engineering applications. In the context of geotechnical engineering and subsurface remediation applications, calcite precipitation can have both positive and negative effects. A range of studies have reported undesirable effects of calcite precipitation associated with well clogging, that is the reduction of hydraulic conductivity around wells. This leads to the need for regular well redevelopment in aquifer storage and recovery applications (Pavelic *et al.* 2007) and reduces the accessible depth of a well for fluids in geothermal applications (Regenspurg *et al.* 2015). Calcite precipitation has also been reported to affect the working lifetime of permeable reactive barriers using Fe^0 (Liang *et al.* 2003). Besides these undesirable effects of calcite precipitation, beneficial effects of calcite precipitation have also been widely explored (DeJong *et al.* 2013). For example, field tests with microbially induced calcite precipitation have demonstrated its potential for bioremediation (Fujita *et al.* 2008, 2010), stabilization of soil (Burbank *et al.* 2011; Gomez *et al.* 2015) and the reduction of liquid permeability (Cuthbert *et al.* 2013; Phillips *et al.* 2016). In many of these studies, the effectiveness of calcite precipitation was monitored by measuring hydraulic pressure, analysing biochemical properties of sampled solution and with cone penetration tests. However, these methods are spatially and temporally limited, expensive and laborious.

Geophysical methods offer the possibility of non-invasive measurements at a range of spatial and temporal scales by using sensors deployed on the boundary of the area of interest (Binley *et al.* 2015). Some studies have used seismic methods for real-time and non-destructive monitoring of calcite precipitation (Mujah *et al.* 2017). However, seismic methods are less suitable for long-term monitoring in field applications because this method requires a lot of *in situ* manual procedures. Wu *et al.* (2010) have shown that the spectral induced polarization (SIP) method also is sensitive to calcite precipitation. Compared to seismic monitoring of calcite precipitation, SIP measurements have the advantage that they are

able to provide a higher spatial and temporal resolution, and additionally are suitable for long term monitoring due to the relatively straightforward automation (Slater & Sandberg 2000). In addition, it has been demonstrated that SIP measurements have unique sensitivity to biogeochemical processes and products with applications to characterize and monitor geochemically and biologically driven processes in the subsurface (Abdel Aal *et al.* 2004; Williams *et al.* 2005; Mellage *et al.* 2018; Saneiyan *et al.* 2019).

SIP measures the complex impedance in the mHz to kHz frequency range by injecting a sinusoidal current with a known frequency and measuring the resulting voltages. The measured complex electrical conductivity is obtained from the complex impedance using a cell constant and can be expressed as:

$$\sigma^*(\omega) = \sigma'(\omega) + i\sigma''(\omega), \quad (1)$$

where i indicates an imaginary number, σ' and σ'' are the real and imaginary part of the electrical conductivity (S m^{-1}) and ω is the angular frequency (rad s^{-1}). In the SIP frequency range, σ' of a porous medium with a non-conducting solid phase is mainly related to electrolyte conduction in the water-filled pore space of the measured sample, whereas σ'' is mainly related to polarization of the measured sample and its relaxation process in an alternating electric field. Schwartz (1962) proposed that this polarization is related to the electric double layer at the solid–fluid interface. Several studies have developed more advanced mechanistic models based on this work (e.g. Lyklema *et al.* 1983; Revil & Glover 1997; Leroy *et al.* 2008). An alternative formulation for the complex electrical conductivity is:

$$\sigma^* = |\sigma| e^{-i\varphi}, \quad (2)$$

where $|\sigma|$ is the conductivity magnitude and φ is the phase shift between the applied current and the resulting measured voltage. The phase is related to σ' and σ'' through:

$$\varphi = \tan^{-1}\left(\frac{\sigma''}{\sigma'}\right) \approx \frac{\sigma''}{\sigma'}, \quad (3)$$

where the approximation is valid for $\varphi < 100$ mrad, which is the case in almost all SIP applications in natural sediments.

The results of the limited number of studies investigating the SIP response of calcite precipitation are not fully consistent (Table 1). Wu *et al.* (2010) mixed two solutions in a column filled with glass beads to induce calcite precipitation and observed a strong increase in σ'' with an increasing amount of calcite precipitation. The maximum σ'' and φ were about 4 mS m^{-1} and 50 mrad, respectively. However, other studies observed considerably weaker SIP responses due to calcite precipitation. Saneiyan *et al.* (2018) induced calcite precipitation by mixing of two saline solutions in a sand column and observed a maximum σ'' of 0.45 mS m^{-1}. Wu *et al.* (2011) used natural groundwater amended with urea to induce calcite precipitation in a column filled with natural sediment. The induced calcite precipitation resulted in an increase in σ'' of about 0.02 mS m^{-1} and a 1 mrad increase in φ. Zhang *et al.* (2012) investigated a column filled with silica gel amended with the urease enzyme, and induced calcite precipitation by injecting urea. In this experiment, σ'' and φ decreased when calcite precipitation was induced. Although the SIP response of calcite precipitation is expected to depend on the amount of calcite precipitation, additional factors controlling the SIP response have not yet been systematically investigated (Wu *et al.* 2010).

It is well known that SIP is determined by the surface chemistry of the investigated sample (Lesmes & Frye 2001; Merriam 2007). Therefore, the relatively large differences in SIP response obtained in previous studies may have been related to different chemical conditions near the precipitated calcite surfaces. Recently, Leroy *et al.* (2017) proposed a mechanistic grain polarization model considering the polarization of the electrical double layer of calcite. Their model predicts that σ'' increases as the surface charge density of the calcite increases, which in turn is controlled by the solute concentration and the equilibrium constants of the complexation reactions at the calcite/water interface as defined in the model of Heberling *et al.* (2014). Leroy *et al.* (2017) parametrized their model using measured outflow data by Wu *et al.* (2010) after the chemical composition of the outflow became roughly constant, and solute concentration was assumed to be homogeneous throughout the column. However, this assumption may not be fully appropriate since calcite precipitation was induced under highly oversaturated conditions in the absence of chemical equilibrium between the solution and the calcite phase. In such a situation, it is likely that the concentration of the outlet solution only partly represents the solute concentration in contact with the calcite. Within this context, the aim of this study is to investigate the sensitivity of the SIP response of calcite to changes in solute concentration using laboratory column experiments.

2 MATERIALS AND METHODS

Laboratory experiments were conducted using an acrylic column with an inner diameter of 3.0 cm and a height of 18 cm (Fig. 1), and the SIP measurement system developed by Zimmermann *et al.* (2008). This SIP system uses four electrode channels. Two channels were connected to porous brass plates at the top and bottom of the column that were used to inject current into the sample. The injected current was generated by applying a sinusoidal voltage wave of ±5 V in the frequency range from 1 Hz to 45 kHz using a function generator (Agilent 33120A, Agilent Technologies, Santa Clara, CA, USA). The amount of injected current was measured using a shunt resistor connected to the top current electrode. The other two channels of the SIP system were connected to two potential electrodes placed at 6.0 and 12.0 cm height between the current electrodes to measure voltages. These electrodes had a diameter of 0.8 cm and were made of brass. Cable glands with an inner diameter of 0.8 cm were used to connect the column and potential electrodes without water leakage. To avoid electrode polarization during the SIP measurements, the potential electrodes were retracted by 1.6 cm (twice the inner diameter of the cable gland) following recommendations of Zimmermann *et al.* (2008) and Huisman *et al.* (2016). The four electrodes were connected to an amplifier unit to minimize load during potential measurements. The measured voltages were digitized with data acquisition cards (NI4472, National Instruments, Austin, TX, USA). The function generator and data acquisition cards were controlled by LabVIEW (National Instruments, Austin, TX, USA).

The column was equipped with two solute injection ports at the bottom and side, and one solute outlet port at the top (see Fig. 1). For the injection port at the side of the column, an additional injection tube was inserted into the sample such that the injection point was in the middle between the potential electrodes. The column was filled with F36 sand (0.09–0.25 mm, Quarzwerke Frechen, Germany) up to 1.4 cm below the top current electrode using a wet-packing procedure. The water-filled space between the sand surface and the top current electrode was used to prevent clogging of the current electrode by calcite precipitation in the flow experiments. Initially, the sample was saturated with 26.2 mM $CaCl_2$ solution (Solution pair 1 in Table 2).

Table 1. Summary of previous researches about SIP response of calcite precipitation in laboratory experiments. Increase in imaginary part of the conductivity and solute concentrations used in the experiments are shown.

Reference	Observed increase in imaginary part of conductivity (mS m^{-1})	Solute concentration
Wu *et al*. (2010)	4	$CaCl_2$: 26.2 mM Na_2CO_3: 29.0 mM
Wu *et al*. (2011)	0.02	Ca^{2+}: 1 mM Total dissolved carbonate: 4 mM
Zhang *et al*. (2012)	Decreased	Ca^{2+}: 10 mM Urea: 10 mM
Saneiyan *et al*. (2018)	0.45	$CaCl_2$: 20 mM Na_2CO_3: 20 mM

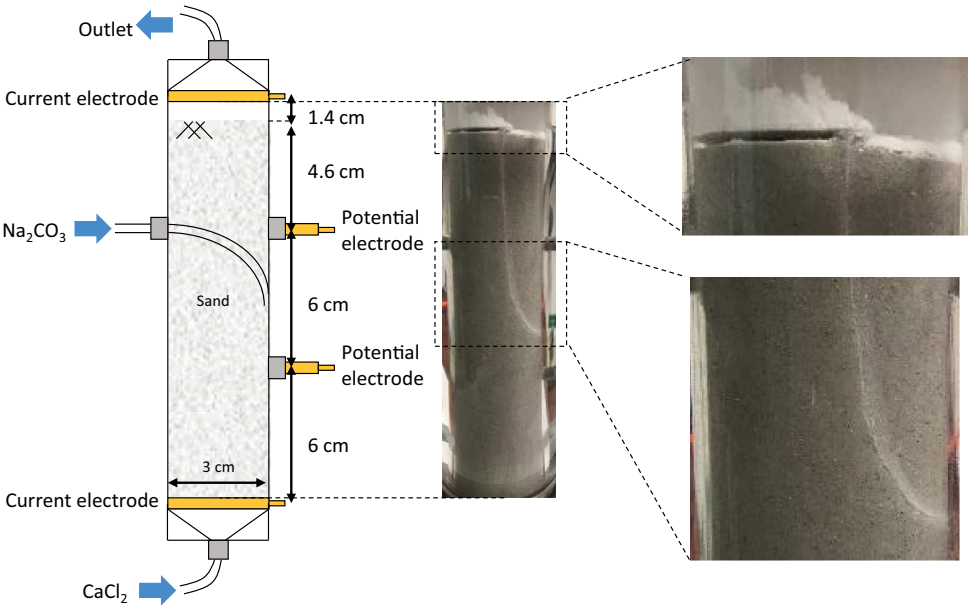

Figure 1. Schematic drawing of the column with electrode positions and a photo of the column at day 12. The injection tube for Na_2CO_3 was bent to inject solution in the middle between the potential electrodes.

Table 2. Electrical conductivity, pH and concentration of injected solution pairs. Solution pair 1 with a saturation index of 3.18 was used to generate calcite precipitation until day 12, and solution pair 2 with a saturation index of 3.18 was used for rest of the experiments.

Solution pair no.		1	2	3	4	5
Saturation index		3.18	3.18	2.85	2.50	2.00
$CaCl_2$	Electrical conductivity (mS cm^{-1})	4.95	4.95	2.69	1.46	0.62
	pH	6.07	6.64	6.76	6.38	6.98
	Concentration (mmol l^{-1})	26.2	26.2	13.6	7.1	2.9
Na_2CO_3	Electrical conductivity (mS cm^{-1})	4.43	4.44	2.51	1.44	0.62
	pH	11.2	11.2	11.2	11.1	11.0
	Concentration (mmol l^{-1})	29.0	29.0	15.1	7.8	3.2
	Injection time in phase II (hr)		3.0	4.0	3.0	3.0

The flow experiments with the sand column were separated in four phases. In phase I, 29.0 mM Na_2CO_3 and 26.2 mM $CaCl_2$ solutions (Solution pair 1 in Table 2) were injected with a flow rate of 2.93 ml hr^{-1}. The $CaCl_2$ solution was injected from the bottom and the Na_2CO_3 solution was injected from the side, which resulted in a clear precipitation front within the sample (see Fig. 1). The solute concentrations and flow rates were selected to be close to the values used in Wu *et al*. (2010). In that study, it was confirmed that the observed precipitation was calcite by direct observation with a scanning electron microscopy. Given the similar experimental conditions, we assumed that the precipitation observed in our experiment also was calcite. The precipitation of calcite is described by

$$Ca^{2+} + CO_3^{2-} = CaCO_3\,(s)\,. \tag{4}$$

The degree of oversaturation can be described by the saturation index SI (Appelo & Postma 2007):

$$SI = \log(IAP/K)\,, \tag{5}$$

where IAP is the ion activity product and K is the solubility product ($10^{-8.48}$ for calcite). For calcite, the IAP is defined as:

$$\mathrm{IAP}_{\mathrm{Calcite}} = a_{\mathrm{Ca}^{2+}}\, a_{\mathrm{CO}_3^{2-}}, \tag{6}$$

where $a_{\mathrm{Ca}^{2+}}$ is the activity of the calcium ion and $a_{\mathrm{CO}_3^{2-}}$ is the activity of the carbonate ion. The saturation indices of the injected solutions (Table 2) were calculated based on chemical specialization by PhreeqC (Parkhurst & Appelo 2013). Throughout all experimental phases, the observed pH of the $CaCl_2$ solution (Table 2) was slightly below the expected pH calculated using PhreeqC (7.0), which indicated that CO_2 from the atmosphere dissolved into the solution. However, PhreeqC calculations showed that the total amount of dissolved CO_2 was less than 0.01 per cent of the carbonate added as Na_2CO_3 in all the solution pairs. In addition, the maximum difference between the measured and calculated pH of the Na_2CO_3 solution was only 0.1. For these reasons, dissolution of the CO_2 into the solutions was ignored in the calculation of the saturation indices. It is important to note that calcite precipitation was expected to be mainly induced in the zone where the two injected solutions mixed. Therefore, the calculated saturation index based on the assumption of two fully mixed solutions may not be fully representative for the conditions near the precipitates since the ongoing calcite precipitation in the reaction front will locally reduce ion activity and the saturation index. In this first experimental phase, SIP measurements were made every 2 d for 12 d in order to investigate the SIP response associated with the development of calcite precipitates in the column. Additionally, the electrical conductivity of the outlet solution was measured every day.

After phase I, three additional experimental phases (phase II to phase IV) were implemented to investigate the effect of solute concentration on the SIP response. Na_2CO_3 and $CaCl_2$ solutions with the same salt concentrations as used in phase I (Solution pair 2 in Table 2) were injected between each of these experimental phases in order to approximately come to the same SIP response as at the end of phase I at the start of phase II–IV. This was only partly successful since the σ'' increased substantially between the start of phase II and III. This likely indicates additional calcite precipitation between phase II and phase III, which is difficult to avoid when working with oversaturated solutions. For this reason, care should be taken when comparing SIP measurements between phases.

In phase II, the injected solutions were increasingly diluted in steps. First, the solution pair with a saturation index of 3.18 (more than 1500 times higher concentration than the equilibrium condition) was injected for 3 hr (solution pair 2 in Table 2), followed by the injection of solution pairs diluted by a factor of 1.9 for the first 2 steps and 2.5 for the last step (solution pair 3–5 in Table 2). The duration of the injection of each solution pair was 3 or 4 hr (Table 2). SIP measurements were made after each dilution step. To limit the amount of additional calcite precipitation in this experimental phase, the entire phase lasted only 13 hr. In order to sufficiently flush the column within the limited available experimental time, the injection rate was increased to 28.2 ml hr^{-1} for both ports. With this higher flow rate, the total volume of the injected solution was at least 3.5 times larger than the pore volume of the sand (48.6 ml). In phase III, the injection of the two solutions was stopped for 50 hr and SIP measurements were made at regular time intervals. In phase IV, the injection rate of the Na_2CO_3 solution was reduced to 45 per cent of the original injection rate (1.31 ml hr^{-1}) for 7 hr. This change in flow rate was expected to shift the position of solute mixing zone away from the original calcite precipitation front and thus change the solute concentration of the water in contact with the precipitated calcite.

Because of the assumed importance of the position of the mixing zone of the two injected solutions, the streamlines and velocity fields within the column in phase I, II and IV were simulated using the open-source simulation platform OpenFOAM® (http://www.openfoam.org). In these simulations, the hydraulic conductivity of the F36 sand was assumed to be 2.0×10^{-2} cm s^{-1} as determined by Koch *et al*. (2011). Porosity was 0.41 (cm^3 cm^{-3}) based on the measured weight of the packed sand.

3 RESULTS AND DISCUSSION

Fig. 2(a) shows the simulated streamlines for the injected Na_2CO_3 and $CaCl_2$ solution in phase I indicating that the two solutions were not fully in contact with each other and thus incompletely mixed, which implies that only a part of the injected solutions reacted within the sand column. It is important to note that this simulation result should only be interpreted in a qualitative manner since the feedback of the calcite precipitation on the flow and the associated reaction kinetics in such a highly oversaturated solution have not been considered here. Fig. 1 shows a photo of the column at the end of phase I (day 12). The white area in the column indicates the calcite precipitation front at the position where the two solutions were expected to mix. The observed shape of the precipitation front was similar to the shape of the boundary between the streamlines of the two injected solutions. Also, it was visually observed that precipitation was strongest just below the injection point (Fig. 1). This is consistent with the low simulated pore water velocity in this area (Fig. 2a), which resulted in the largest residence time of the injected Na_2CO_3 solution. Additional calcite precipitation was observed on the surface of the sample, which also emphasizes the incomplete mixing in the sand column (Fig. 1).

The conductivity of the outlet solution varied between 2.83 and 2.92 mS cm^{-1} except for the first day where it was 3.73 mS cm^{-1}. A solution in equilibrium with calcite was calculated to have an electrical conductivity of 2.95 mS cm^{-1} using PhreeqC, which is near the observed conductivity values. However, it should be noted that the outlet solution likely did not represent the solute concentration within the SIP measurement zone between the potential electrodes, because the injected solutions were only fully mixed in the water layer above the sample material as indicated by the calcite precipitation on the surface of the sample (Fig. 1) and by the simulated streamlines (Fig. 2).

Fig. 3 shows the development of σ' and σ'' during phase I. For the initial conditions at day 0, the cementation factor m in Archie's law (Archie 1942) was calculated to be 1.5 using:

$$\lim_{\sigma_s \to 0} \left(\frac{\sigma_w}{\sigma} \right) = \phi^{-m}, \tag{7}$$

where σ_s is the surface conductivity, σ_w is the solution conductivity of the $CaCl_2$ solution in the column (4.95 mS cm^{-1}), σ is the real part of the conductivity at 1 kHz (1.33 mS cm^{-1}), and ϕ is the porosity (0.41 cm^3 cm^{-3}). σ' decreased between day 0 and day 2 after the injection of the Na_2CO_3 solution was initiated. This was expected because the conductivity of the Na_2CO_3 solution was smaller than the conductivity of the $CaCl_2$ solution that was initially present (Table 2). Between day 2 and day 4, σ' did not change significantly. The porosity ϕ at day 2 and day 4 can be estimated by assuming that σ_w can be approximated by the average conductivity of the injected solutions and assuming that m is constant, which is reasonable given that m is only related to the shape of the grains (Sen *et al.* 1981;

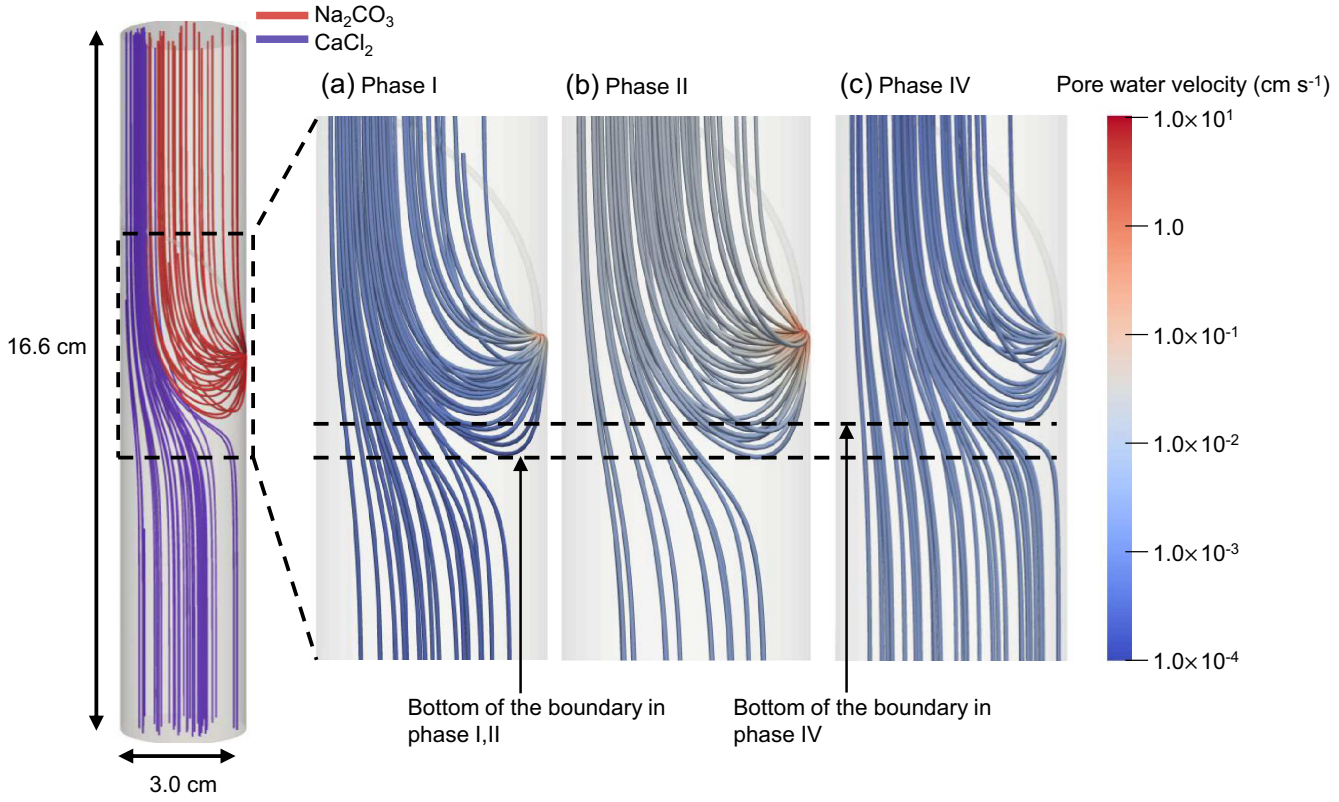

Figure 2. Simulated streamlines of Na_2CO_3 and $CaCl_2$ solution in the entire column and a close-up of the area near the injection tube for (a) phase I, (b) phase II and (c) phase IV.

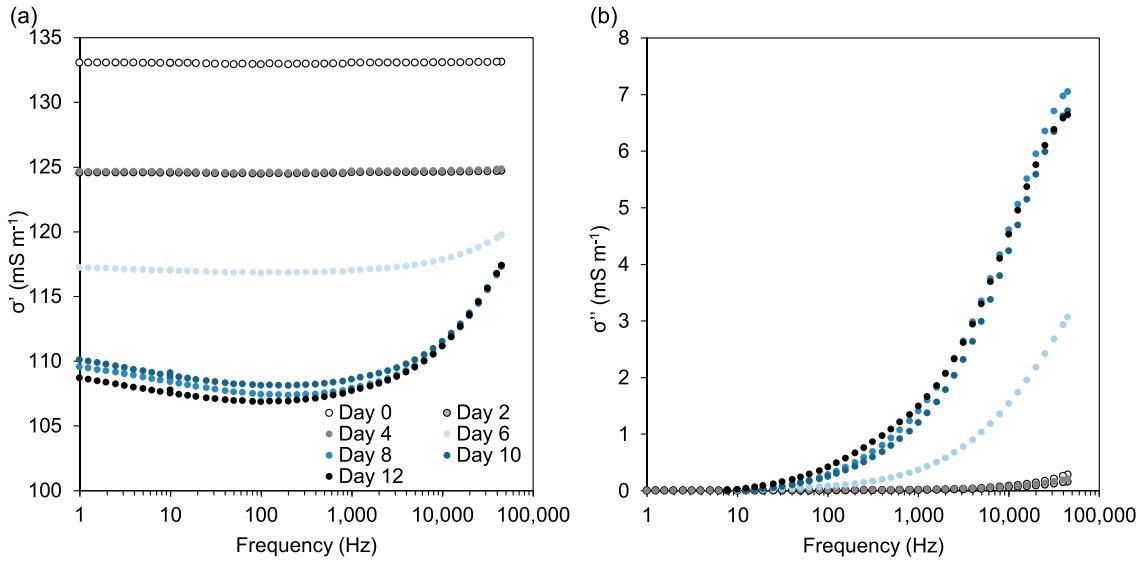

Figure 3. Change in (a) σ' and (b) σ'' caused by calcite precipitation during the first 12 d of phase I. Open symbols represent the measured values in the initial condition before starting the injection.

Bussian 1983). No significant changes in porosity were obtained using this approach.

For the first 4 d, σ'' was almost constant although calcite precipitation was observed visually. The lack of change in σ'' and estimated porosity perhaps suggests that the amount of calcite precipitation may not have been sufficient to generate a SIP response in the early stages of the experiment as will be discussed below. The lack of response may also have been affected by the initial formation of meta-stable amorphous calcium carbonate, which is reportedly first formed when $CaCl_2$ and Na_2CO_3 solutions with a saturation index larger than 2.1 are mixed (Rodriguez-Navarro *et al.* 2016). This was confirmed for the two solutions used in phase I by mixing them in a beaker. This resulted in a white opaque solution that was created within some minutes after mixing. This metastable amorphous

phase disappeared again after some hours, after which the solution became transparent again. Kinetic effects directly associated with calcite precipitation may also have played a role in the weak SIP response in the first days. It has been shown that the growth of calcite crystals highly depends on the availability of nucleation sites on calcite surfaces, because calcite crystals mainly grow through the attachment of ions or amorphous calcium carbonate to the surface of calcite (Morse *et al.* 2007; Rodriguez-Navarro *et al.* 2016). For all these reasons, the growth rate of calcite may have been small in the first days of our experiment.

σ' slightly decreased between day 4 to day 8, and σ'' markedly increased in this period. The observed strong increase in σ'' is consistent with the results presented in Wu *et al.* (2010), who mixed $CaCl_2$ and Na_2CO_3 solutions with the same concentrations as used here in a column filled with glass beads. After day 8, σ' and σ'' remained almost constant despite continuous input of solutes, indicating that the amount of calcite was almost constant within the measurement zone. This may be due to the limited further mixing and reaction between the injected solutions in the measurement zone because of the growth of the calcite precipitation within the pore space. This feedback between precipitation and reaction rate was already observed in a previous microfluidic experiment (Zhang *et al.* 2010).

In phase II, the column was flushed with solutions with a different saturation index (Solution pair 2–5 in Table 2) and a higher injection rate. Fig. 2(b) shows the simulated streamlines and pore water velocity in phase II (again neglecting effects of calcite precipitation on the flow field). A comparison with the simulated streamlines of phase I (Fig. 2a) shows that the boundary between the injected Na_2CO_3 and $CaCl_2$ solutions did not change between these two experimental phases. Obviously, the pore water velocity was higher in phase II due to the higher injection rate. These simulation results suggest that the calcite precipitation generated in phase I was expected to be in contact with the injected Na_2CO_3 and $CaCl_2$ solutions in phase II. This was further confirmed by the SIP measurements for solution pair 2, where it was found that the increase in injection rate only resulted in a maximum decrease of 1.2 mS m^{-1} at 40 kHz for σ'' within the first hour. This initial small decrease may be because some calcite precipitation was dislodged and flushed out of the sample due to the increased shear stress associated with higher flow velocities.

When the column was flushed with solution pairs with decreasing saturation index, σ' and σ'' both decreased (Fig. 4). The decrease in σ' is directly related to the decrease in the electrical conductivity of the two solutions (Table 2). In addition, it is well known that σ'' depends strongly on solution conductivity for several geological media (Revil & Skold 2011; Weller & Slater 2012). The relationship between σ'' and the electrical conductivity of the solution (σ_w) is shown in Fig. 5 for three different frequencies. As the reaction kinetics of the calcite precipitation were not clear in our experiment, σ_w was calculated by assuming that the reaction rate is either very slow (Fig. 5a) or very fast (Fig. 5b). In the first case, σ_w equals the average electrical conductivity of the injected solution. In the second case, the σ_w was calculated using PhreeqC assuming that the solution is in equilibrium with calcite. In both cases, a simple power-law function was fitted to the observed σ'' (1, 10 and 45 kHz) and σ_w:

$$\sigma''(f) = a(\sigma_w)^b, \tag{8}$$

where a and b are fitting parameters (Weller & Slater 2012). The b value in the fitted power law varied from 0.83 to 1.05 with increasing frequency. Weller & Slater (2012) reported b values for sand and sandstone that ranged from 0.10 to 0.64, with a mean value of 0.34 for solute conductivities less than 1000 mS m^{-1}. Although the values of Weller & Slater (2012) were obtained for a lower frequency (less than 30 Hz), the larger b values in our experiment suggest that the SIP response of calcite has a stronger dependence on the solute conductivity than sand and sandstone. It is important to note that the petrophysical model from Weller & Slater (2012) is for equilibrium conditions, while our system is not in equilibrium and precipitation of calcite is occurring continuously during the experiment.

When the injection of both solutions was stopped in phase III, the σ' varied only ±5 per cent and showed an initial increase and a subsequent small decrease (Fig. 6a). This change was much smaller than the difference between σ' at the start and at the end of phase III. Thus, this change in σ' was not attributed to the formation of calcite precipitation, but to a moderate change in solute concentration. Considering that σ' varied only ±5 per cent, only a small part of the ions in the column could have been consumed due to calcite precipitation after flow was stopped. Nevertheless, σ'' significantly decreased over time (Fig. 6b) albeit with a decreasing rate as shown exemplary in Fig. 7 for a frequency of 1 kHz. We hypothesize that this strong decrease in σ'' is related to a decrease of the solute concentration in contact with the calcite in the precipitation front. When injection and flow was stopped, calcite precipitation continued and the concentration of Ca^{2+} and carbonate species (HCO_3^- and CO_3^{2-}) in the mixing zone decreased, whereas Na^+ and Cl^- did not react. Such a decrease in the concentration of Ca^{2+} and carbonate species will lead to a decrease in σ'' as already shown in phase II of the experiment. Interestingly, this decrease in σ'' is fully reversible since the σ'' returned to very similar values 21 hr after injection was started again (Fig. 6). It should be noted that σ'' continued decreasing even 50 hr after stopping the injection. This long duration probably reflects the slow change in solute concentration near the calcite precipitation as a result of a balance between the kinetics of the precipitation reaction and the continuous supply of solutes from outside the mixing zone through diffusion. This interpretation of the experimental data suggests that it is important to consider the solute concentration in contact with calcite, and not the solute concentration in the bulk water or the outflow. While direct evidence is absent to support this interpretation, it is speculated that the concentration of calcium and carbonate near the calcite surface have a large effect on the surface charge properties of calcite and thus on σ''.

In phase IV, the injection rate of the Na_2CO_3 solution was reduced. Compared to the streamlines in phase I and II (Figs 2a and b), this reduction shifted the mixing zone upward and slightly to the right (Fig. 2c). σ' increased slightly during phase IV (Fig. 8a) because the more conductive $CaCl_2$ solution occupied a larger volume of the sample. Again, σ'' was found to decrease strongly (Fig. 8b) despite the slight increase in mean electric conductivity of the pore water. These results apparently contradict the results of phase II and III. However, it is important to realize that the pore water solution in contact with the calcite in phase IV was probably different from that in phase II and III because the mixing zone was moved as shown in the simulation results (Fig. 2). Part of the calcite precipitated before phase IV is now only in contact with $CaCl_2$ solution, which has larger σ_w, lower pH, higher concentration of Ca^{2+} and lower concentration of carbonate species than the Na_2CO_3 solution. The observed decrease in σ'' can thus reasonably be explained by assuming that changes in solute concentration of the water in contact with the calcite affected the surface chemistry of the calcite. Although previous studies have shown a large variation in pH dependence of surface charges of calcite (Wolthers *et al.* 2008), it is generally

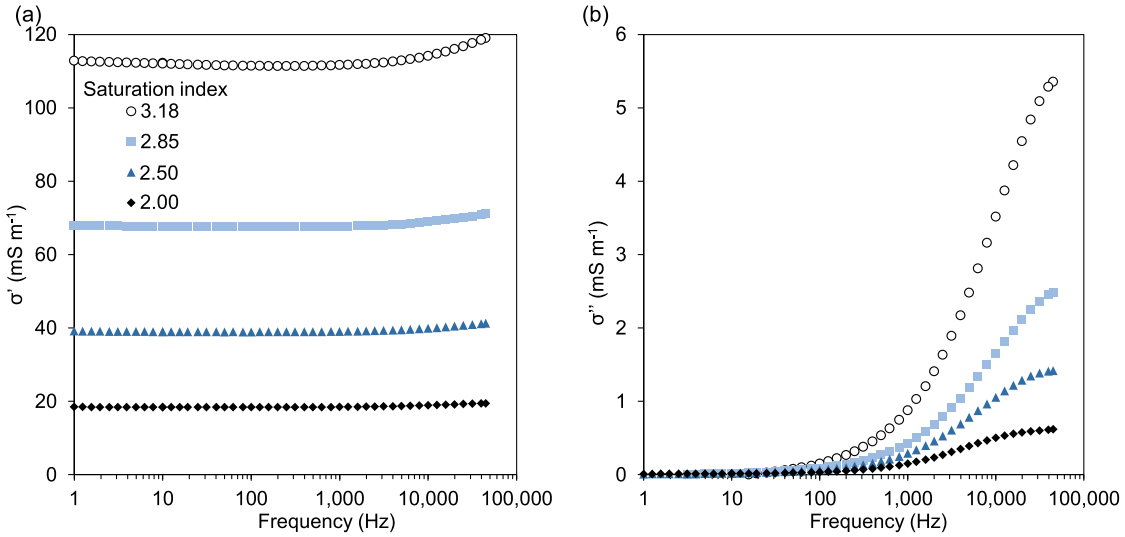

Figure 4. Change in (a) σ' and (b) σ'' when the column was flushed with solution pairs with different saturation index (solution pair 2–5 in Table 1) in phase II.

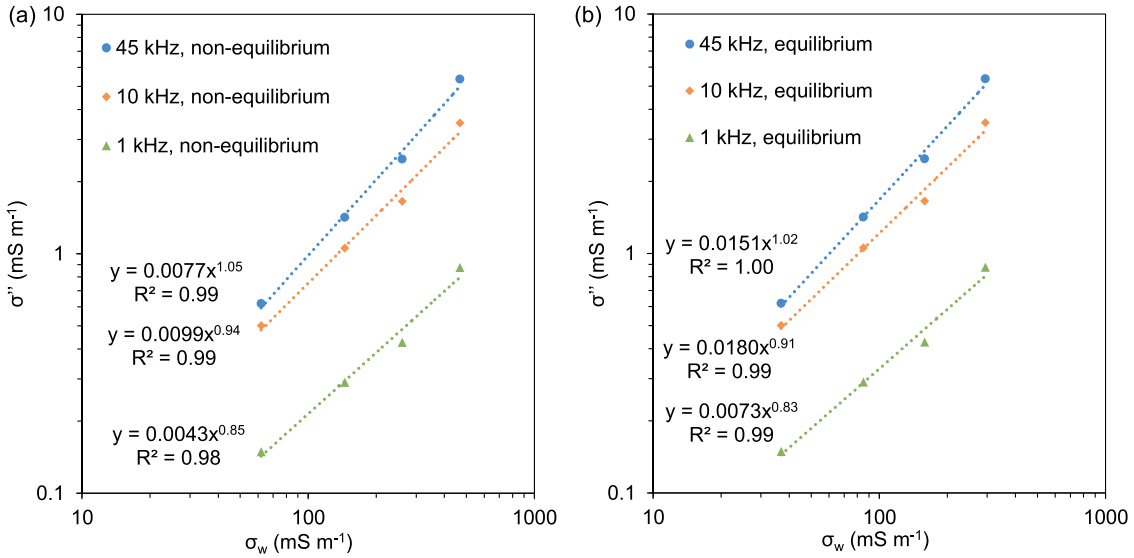

Figure 5. Relationship between σ_w and σ'' in phase II for different frequencies by assuming that the injected solutions were (a) reacting slowly and thus not in equilibrium with calcite and (b) reacting quickly and thus in equilibrium with calcite. The associated fits of eq. (7) to the measured values are also presented.

agreed that a decreasing pH leads to an increase of protonation on the calcite surface. For example, Eriksson *et al.* (2007) showed that the net proton charge on the calcite surface strongly increased below a pH of 8. Since the pH of the $CaCl_2$ solution in our experiment was 6.64, this increase in proton charge may have decreased the number of negatively charged sites on the calcite surface and thus decreased the SIP response (Philippe Leroy *et al.* 2017). Because the calcite surface charge and the solute concentration near the precipitation front cannot directly be observed in our experimental setup, this will need to be examined in more detail in future work.

The results of the flow experiments in phase II, III and IV qualitatively showed that the SIP response of calcite precipitation depended on the solute concentration near the zone of calcite precipitation. A more quantitative analysis does not seem meaningful. One reason is that there was unexpected increase in maximum σ'' between the start of the phase II and III (3.5 mS m^{-1}) and between the start of phase III and IV (0.3 mS m^{-1}). This suggests that the amount of calcite precipitation increased after the start of phase II. It should be noted that σ'' decreased in each phase, thus the variation in σ'' was not attributed to the amount of calcite but to the solute concentration. The other reason is the unknown spatial distribution and kinetics of calcite precipitation in combination with the heterogeneity of the flow velocity field in the column. The most promising way forward towards a quantitative understanding of the SIP response of calcite precipitation requires a combination of reactive transport modelling with more advanced experimental setups that allow determining the distribution of calcite precipitation and solute concentration (e.g. a 2-D milli-fluidic measurement cell).

Despite the qualitative nature of the insights obtained here, it is interesting to evaluate the results of previous studies (Table 1) on the SIP response of calcite precipitation within the light of the current results. For example, Wu *et al.* (2011), Zhang *et al.* (2012)

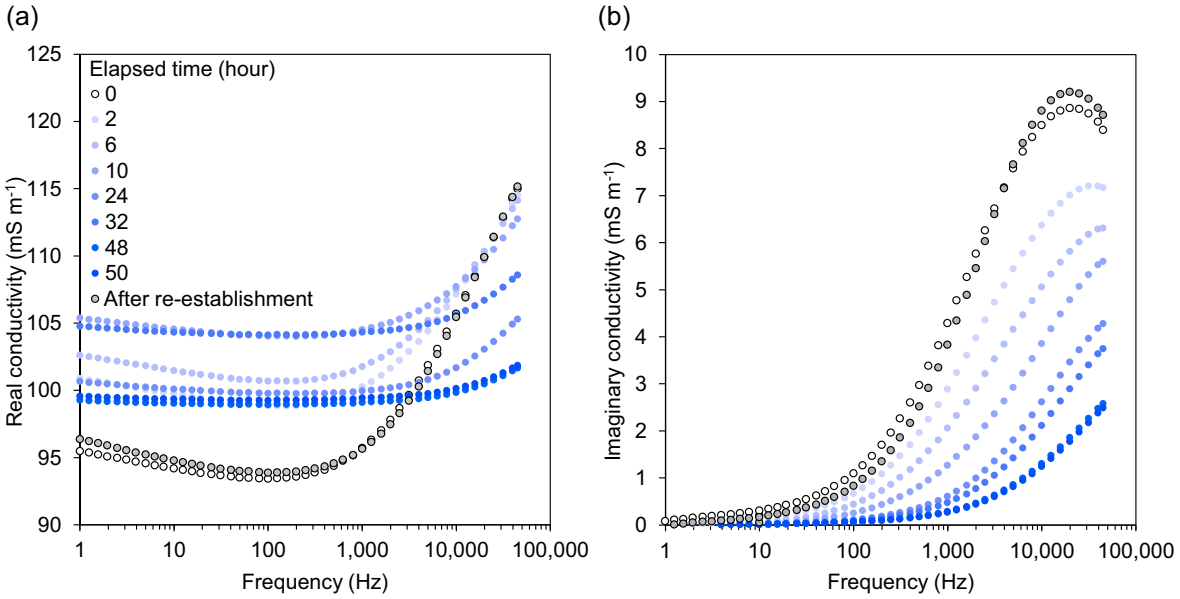

Figure 6. The development of (a) σ' and (b) σ'' as a function of time when solute injection was stopped in phase III. Open symbols represent the measured values before flow was stopped at $t = 0$ hr. Darker colour represents longer elapsed time. The grey symbols represent measured values after re-establishment of the condition at the start of this phase by injecting solution pair 2 of Table 1.

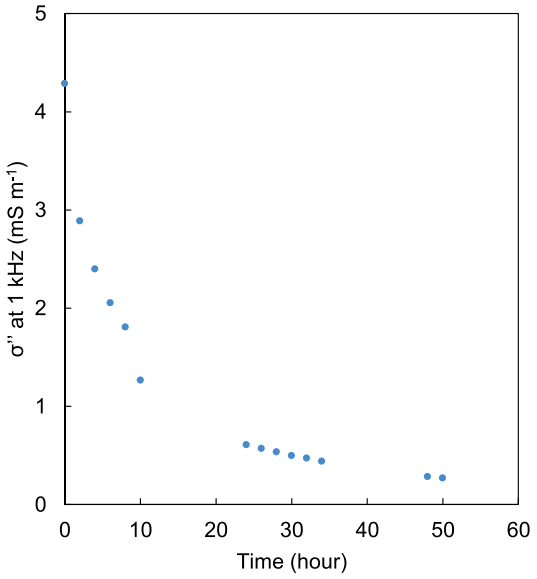

Figure 7. Change in σ'' at 1 kHz over time after stopping injection of both $CaCl_2$ and Na_2CO_3 solution in phase III.

and Saneiyan *et al*. (2018) all reported significantly smaller SIP responses than presented in this study and Wu *et al*. (2010). Although part of the differences is certainly due to the different amounts of calcite precipitation in these studies, it is now clear that the concentration of Ca^{2+} and the carbonate species also need to be considered. In Wu *et al*. (2011), the Ca^{2+} and the total dissolved carbonate concentration in the influent solution were about 1 and 4 mM, respectively. These concentrations were much lower than the concentration of Ca^{2+} (29 mM) and dissolved carbonate concentration (26.2 mM) in the injected solutions in phase I of our study. Therefore, the concentration of Ca^{2+} and carbonate species in Wu *et al*. (2011) may not have been enough to generate a strong SIP response even in the presence of sufficient calcite precipitation. In Zhang *et al*. (2012), the concentration of Ca^{2+} and urea were 10 mM. Considering that the urease enzyme produces dissolved carbonate due to the decomposition of urea, the maximum concentration of carbonate species was 10 mM. However, Ca^{2+} adsorption on silica gel was strong as described in Zhang *et al*. (2012). Thus, the concentration of Ca^{2+} in the solution in contact with the precipitated calcite was probably not high enough to generate a significant SIP response. In the column experiment by Saneiyan *et al*. (2018), the distribution of calcite precipitation and solute concentration were not clear, and it may be possible that the calcite precipitation did not overlap with the mixing zone of the solutions. Based on this short survey of previous work, it seems likely that some of the observed weak SIP responses may be attributed to lower concentrations of Ca^{2+} and carbonate species in the solution in contact with the precipitated calcite in addition to potentially different amounts of calcite precipitation.

4 CONCLUSIONS

In this study, calcite precipitation was induced in a column by mixing Na_2CO_3 and $CaCl_2$ solutions and SIP measurements were made during a flow experiment composed of four phases. In phase I, a significant SIP response was observed due to the calcite precipitation induced in the column. In phase II, the column was flushed with solutions with a different saturation index and thus a different pore water conductivity. The results suggested that the SIP response of calcite has a stronger dependence on the solution conductivity than sand and sandstone. When the injection of both solutions was stopped in phase III, σ'' decreased. This was attributed to a decrease in the concentration of Ca^{2+} and CO_3^{2-} in contact with the calcite in the precipitation front. In phase IV, the injection rate of the Na_2CO_3 solution was reduced to shift the mixing zone away from the calcite precipitation front. Therefore, part of the calcite precipitation front generated in phase I was only in contact with the $CaCl_2$ solution. Despite a bulk increase in the electric conductivity of the pore water due to the more conductive $CaCl_2$ solution, it was observed that σ''

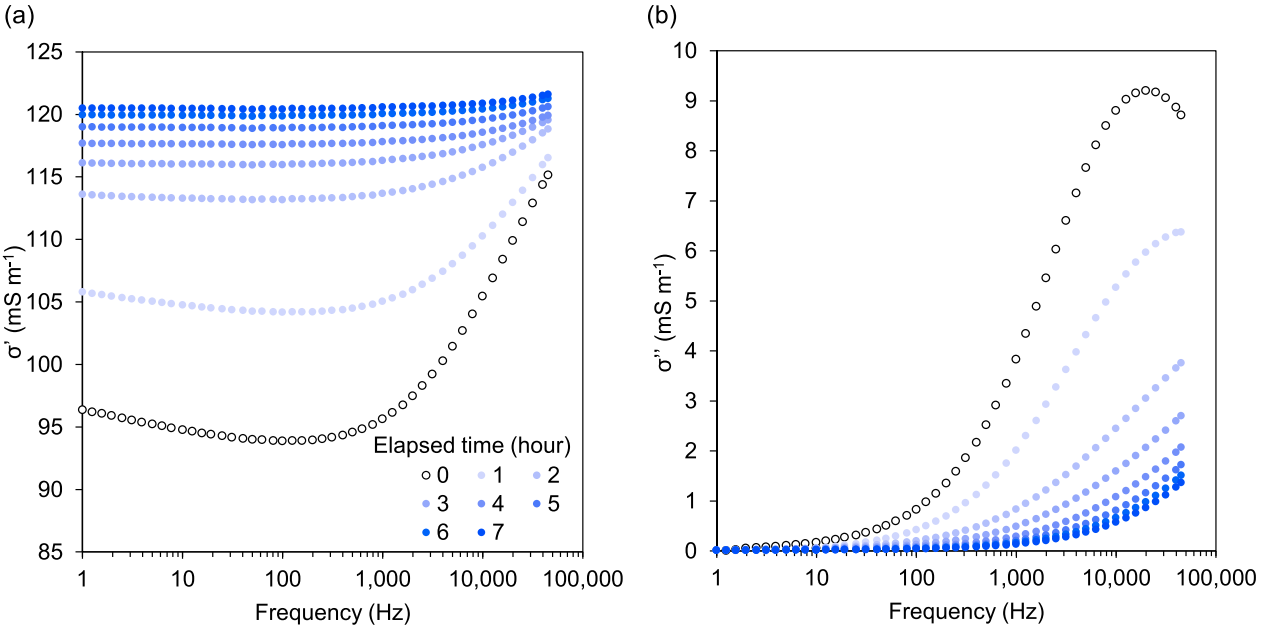

Figure 8. Development of (a) σ' and (b) σ'' when the injection rate of the Na_2CO_3 solution was reduced relative to that of the $CaCl_2$ solution. Darker colour represents longer elapsed time.

decreased. This was attributed to interactions between solute concentration and surface chemistry of the calcite. The experimental results presented here clearly highlighted the complex dependency of the SIP response of calcite precipitation on solute concentration. Based on our results, the previously observed relatively weak SIP responses of calcite precipitation (Wu *et al.* 2011; Zhang *et al.* 2012; Saneiyan *et al.* 2018) may be related to lower concentrations of Ca^{2+} and carbonate species in the solution in contact with calcite in addition to variable amounts of calcite precipitation. Future work should focus on obtaining a more quantitative understanding of the relationship between surface chemistry of calcite and SIP response. For this purpose, it is important to quantify how solute concentration affects the SIP response of calcite precipitation, which can only be obtained by a combination of advanced experimental set-ups, spatially resolved reactive transport modelling and deterministic modelling of the SIP response.

ACKNOWLEDGEMENTS

Funding for this study was provided by European Union's Horizon 2020 research and innovation programme under the Marie Sklodowska-Curie Grant Agreement N°722028 to the project entitled 'ENIGMA (European training Network for *In situ* imaGing of dynaMic processes in heterogeneous subsurfAce environments)'. Yuxin Wu acknowledges the support from the U.S. Department of Energy, Office of Science, Office of Basic Energy Sciences, Chemical Sciences, Geosciences and Biosciences Division, through its Geoscience program at LBNL under Contract DE-AC02-05CH11231.

REFERENCES

Abdel Aal, G.Z., Atekwana, E.A., Slater, L.D. & Atekwana, E.A., 2004. Effects of microbial processes on electrolytic and interfacial electrical properties of unconsolidated sediments, *Geophys. Res. Lett.,* **31,** doi:10.1029/2004GL020030.

Appelo, C.A.J. & Postma, D., 2007. *Geochemistry, Groundwater and Pollution,* 2nd edn, Balkema Publishers.

Archie, G.E., 1942. The electrical resistivity log as an aid in determining some reservoir characteristics, *Trans. AIME,* **146,** 54–62.

Binley, A., Hubbard, S.S., Huisman, J.A., Revil, A., Robinson, D.A., Singha, K. & Slater, L.D., 2015. The emergence of hydrogeophysics for improved understanding of subsurface processes over multiple scales, *Water Resour. Res.,* **51,** 3837–3886.

Burbank, M.B., Weaver, T.J., Green, T.L., Williams, B.C. & Crawford, R.L., 2011. Precipitation of calcite by indigenous microorganisms to strengthen liquefiable soils, *Geomicrobiol. J.,* **28,** 301–312.

Bussian, A.E., 1983. Electrical conductance in a porous medium, *Geophysics,* **48,** 1258–1268.

Cuthbert, M.O., McMillan, L.A., Handley-Sidhu, S., Riley, M.S., Tobler, D.J. & Phoenix, V.R., 2013. A field and modeling study of fractured rock permeability reduction using microbially induced calcite precipitation, *Environ. Sci. Technol.,* **47,** 13637–13643.

DeJong, J.T. *et al.*, 2013. Biogeochemical processes and geotechnical applications: progress, opportunities and challenges, *Géotechnique,* **63,** 287–301.

Eriksson, R., Merta, J. & Rosenholm, J.B., 2007. The calcite / water interface I. Surface charge in indifferent electrolyte media and the influence of low-molecular-weight polyelectrolyte, *J. Colloid Interface Sci.,* **313,** 184–193.

Fujita, Y., Taylor, J.L., Gresham, T.L.T., Delwiche, M.E., Colwell, F.S., Mcling, T.L., Petzke, L.M. & Smith, R.W., 2008. Stimulation of microbial urea hydrolysis in groundwater to enhance calcite precipitation, *Environ. Sci. Technol.,* **42,** 3025–3032.

Fujita, Y., Taylor, J.L., Wendt, L.M., Reed, D.W. & Smith, R.W., 2010. Evaluating the potential of native ureolytic microbes to remediate a90Sr contaminated environment, *Environ. Sci. Technol.,* **44,** 7652–7658.

Gomez, M.G., Martinez, B.C., DeJong, J.T., Hunt, C.E., deVlaming, L.A., Major, D.W. & Dworatzek, S.M., 2015. Field-scale bio-cementation tests to improve sands, *Proc. Inst. Civ. Eng. - Gr. Improv.,* **168,** 206–216.

Heberling, F. *et al.*, 2014. Applied geochemistry reactivity of the calcite–water-interface, from molecular scale processes to geochemical engineering, *Appl. Geochem.,* **45,** 158–190.

Huisman, J.A., Zimmermann, E., Esser, O., Haegel, F.-H., Treichel, A. & Vereecken, H., 2016. Evaluation of a novel correction procedure to remove

electrode impedance effects from broadband SIP measurements, *J. Appl. Geophys.,* **135,** 466–473.

Koch, K., Kemna, A., Irving, J. & Holliger, K., 2011. Impact of changes in grain size and pore space on the hydraulic conductivity and spectral induced polarization response of sand, *Hydrol. Earth Syst. Sci.,* **15,** 1785–1794.

Leroy, P., Revil, A., Kemna, A., Cosenza, P. & Ghorbani, A., 2008. Complex conductivity of water-saturated packs of glass beads, *J. Colloid Interface Sci.,* **321,** 103–117.

Leroy, P., Li, S., Jougnot, D., Revil, A. & Wu, Y., 2017. Modelling the evolution of complex conductivity during calcite precipitation on glass beads, *Geophys. J. Int.,* **209,** 123–140.

Lesmes, D.P. & Frye, K.M., 2001. Influence of pore fluid chemistry on the complex conductivity and induced polarization responses of Berea sandstone, *J. geophys. Res.,* **106,** 4079–4090.

Liang, L., Sullivan, A.B., West, O.R., Moline, G.R. & Kamolpornwijit, W., 2003. Predicting the precipitation of mineral phases in permeable reactive barriers, *Environ. Eng. Sci.,* **20,** doi:10.1089/109287503770736159.

Lyklema, J., Dukhin, S.S. & Shilov, V.N., 1983. The relaxation of the double layer around colloidal particles and the low-frequency dielectric dispersion, *J. Electroanal. Chem. Interfacial Electrochem.,* **143,** 1–21.

Mellage, A., Smeaton, C.M., Furman, A., Atekwana, E.A., Rezanezhad, F. & Van Cappellen, P., 2018. Linking spectral induced polarization (SIP) and subsurface microbial processes: results from sand column incubation experiments, *Environ. Sci. Technol.,* **52,** 2081–2090.

Merriam, J.B., 2007. Induced polarization and surface electrochemistry, *Geophysics,* **72,** 157–166.

Morse, J.W., Arvidson, R.S. & Lüttge, A., 2007. Calcium carbonate rormation and cissolution, *Chem. Rev.,* **107,** 342–381.

Mujah, D., Shahin, M.A. & Cheng, L., 2017. State-of-the-art review of ciocementation by microbially induced calcite precipitation (MICP) for soil stabilization, *Geomicrobiol. J.,* **34,** 524–537.

Parkhurst, D.L. & Appelo, C.A.J., 2013. Description of input and examples for PHREEQC Version 3—a computer program for specialization, batch-reaction, one-cimensional transport, and inverse geochemical calculations, *U.S. Geol. Surv. Tech. Methods,* B. 6, chapter A43, 497p, doi:10.1016/0029-6554(94)90020-5.

Pavelic, P., Dillon, P.J., Barry, K.E., Vanderzalm, J.L., Correll, R.L. & Rinck-Pfeiffer, S.M., 2007. Water quality effects on clogging rates during reclaimed water ASR in a carbonate aquifer, *J. Hydrol.,* **334,** 1–16.

Phillips, A.J. *et al.*, 2016. Fracture sealing with microbially-induced calcium carbonate precipitation: a field study, *Environ. Sci. Technol.,* **50,** 4111–4117.

Regenspurg, S. *et al.*, 2015. Mineral precipitation during production of geothermal fluid from a Permian Rotliegend reservoir, *Geothermics,* **54,** 122–135.

Revil, A. & Glover, P.W.J., 1997. Theory of ionic-surface electrical conduction in porous media, *Phys. Rev. B,* **55,** 1757–1773.

Revil, A. & Skold, M., 2011. Salinity dependence of spectral induced polarization in sands and sandstones, *Geophys. J. Int.,* **187,** 813–824.

Rodriguez-Navarro, C., Cara, A.B., Elert, K. & Putnis, C.V., 2016. Direct nanoscale imaging reveals the growth of calcite crystals via amorphous nanoparticles, *Cryst. Growth Des.,* **16,** 1850–1860.

Saneiyan, S., Ntarlagiannis, D., Ohan, J., Lee, J., Colwell, F. & Burns, S., 2019. Induced polarization as a monitoring tool for in-situ microbial induced carbonate precipitation (MICP) processes, *Ecol. Eng.,* **127,** 36–47.

Saneiyan, S., Ntarlagiannis, D., Werkema, D.D. & Ustra, A., 2018. Geophysical methods for monitoring soil stabilization processes, *J. appl. Geophys.,* **148,** 234–244.

Schwarz, G., 1962. A theory of the low-frequency dielectric dispersion of colloidal particles in electrolyte solution, *J. Phys. Chem.,* **66,** 2636–2642.

Sen, P.N., Scala, C. & Cohen, M.H., 1981. A self-similar model for sedimentary rocks with application to the dielectric constant of fused glass beads, *Geophysics,* **46,** 781–795.

Slater, L.D. & Sandberg, S.K., 2000. Resistivity and induced polarization monitoring of salt transport under natural hydraulic gradients, *Geophysics,* **65,** 408–420.

Weller, A. & Slater, L., 2012. Salinity dependence of complex conductivity of unconsolidated and consolidated materials: comparisons with electrical double layer models, *Geophysics,* **77,** D185–D198.

Williams, K.H., Ntarlagiannis, D., Slater, L.D., Dohnalkova, A., Hubbard, S.S. & Banfield, J.F., 2005. Geophysical imaging of stimulated microbial biomineralization, *Environ. Sci. Technol.,* **39,** 7592–7600.

Wolthers, M., Charlet, L. & Van Cappellen, P., 2008. The surface chemistry of divalent metal carbonate minerals; a critical assessment of surface charge and potential data using the charge distribution multi-site ion complexation model, *Am. J. Sci.,* **308,** 905–941.

Wu, Y. *et al.*, 2011. Geophysical monitoring and reactive transport modeling of ureolytically-driven calcium carbonate precipitation, *Geochem. Trans.,* **12,** doi:10.1186/1467-4866-12-7.

Wu, Y., Hubbard, S., Williams, K.H. & Ajo-Franklin, J., 2010. On the complex conductivity signatures of calcite precipitation, *J. geophys. Res.,* **115,** G00G04, doi:10.1029/2009JG001129.

Zhang, C., Ntarlagiannis, D., Slater, L. & Doherty, R., 2010. Monitoring microbial sulfate reduction in porous media using multipurpose electrodes, *J. geophys. Res.,* **115,** 1–11.

Zhang, C., Slater, L., Redden, G., Fujita, Y., Johnson, T. & Fox, D., 2012. Spectral induced polarization signatures of hydroxide adsorption and mineral precipitation in porous Media, *Environ. Sci. Technol.,* **46,** 4357–4364.

Zimmermann, E., Kemna, A., Berwix, J., Glaas, W., Münch, H.M. & Huisman, J.A., 2008. A high-accuracy impedance spectrometer for measuring sediments with low polarizability, *Meas. Sci. Technol.,* **19,** 1–9.